Available online at www.sciencedirect.com
SCIENCE DIRECT®
Catalysis Today 98 (2004) 431–439
CATALYSIS TODAY
www.elsevier.com/locate/cattod

Photocatalytic degradation of orange II by TiO_2 catalysts supported on adsorbents

A. Bhattacharyya, S. Kawi, M.B. Ray*

Department of Chemical and Biomolecular Engineering, National University of Singapore, 4 Engineering Drive 4, Singapore 117576, Singapore

Available online 27 September 2004

Abstract

TiO_2 mediated semiconductor photocatalysis is an established advanced oxidation process for the treatment of contaminated aqueous and gaseous streams. However, TiO_2 exhibits low adsorption ability, especially for non-polar substances due to its polar structure. Low adsorption ability of non-porous TiO_2 particles can be improved by surface augmentation using inert supports. In this work, TiO_2 was impregnated on three different kinds of adsorbents, mesoporous (MCM-41), microporous (β-zeolite) and pillared structure (montmorillonite) where different loadings (10–80%) of TiO_2 were obtained using sol–gel method. The catalysts were characterized by several analytical techniques including XRD, SEM–EDX, XPS, and BET analyzer. Subsequent to the dark adsorption studies, photocatalytic efficiency of the supported catalysts was evaluated using an azo-dye, orange II in water as model compound under different operating conditions. All supported catalysts exhibit good photodegradation efficiency of orange II, and their overall removal efficiency was always better than that of bare TiO_2 produced by the sol–gel method and commercial catalyst, Degussa-P25.

Keywords: Adsorbent; Anatase; Photocatalytic degradation; Sol–gel; Supported TiO_2

1. Introduction

Advanced oxidation processes (AOPs) are effective remediation and treatment methods due to their ability of complete degradation of wide variety of organic pollutants and microbial substances. TiO_2 induced photocatalysis is an established AOP for the treatment of contaminated air and water streams, which is evident from many publications in this area over the last two decades [1–3]. However, there are certain limitations of using bare TiO_2 in photocatalytic reactors. For example, due to small size (about 4–30 nm) TiO_2 aggregates rapidly in a suspension loosing its effective surface area as well as the catalytic efficiency. Being non-porous, TiO_2 exhibits low adsorption ability for the pollutants [4], especially for the non-polar organic compounds due to its polar surface [5,6]. Immobilizing TiO_2 on substrates such as glass matrix, optical fiber and stainless steel plate eliminates the problem of agglomeration, although the photocatalytic efficiency of immobilized TiO_2 is less than the suspended TiO_2 particles [7]. Besides, the specific surface area also decreases due to the fixing of the TiO_2 on non-porous supports reducing the adsorption capacity. For photocatalytic decomposition of a target compound, adsorption of it on the TiO_2 surface is essential prior to the surface reaction. Furthermore, organic pollutants generally occur in low concentrations (ppm level or below) and pre-concentration of the substrates on the surface where photons are adsorbed is a desirable feature for effective photodegradation.

In recent years, attempts have been made to support fine TiO_2 on porous adsorbent materials like silica [8–11], alumina [12,13], activated carbon [14–16], clay and zeolites [5,7,17–19]. TiO_2 supported on adsorbent provides higher specific surface area and facilitates more effective adsorption sites than bare TiO_2 [5,7,14,20,21]. The enhanced decomposition rates are attributed to the increased condensation of organic substrates on the supported catalyst by adsorption and the reduced electron–hole recombination process on the surface

* Corresponding author. Tel.: +65 6874 2885; fax: +65 6779 1936.
E-mail address: cheraym@nus.edu.sg (M.B. Ray).

0920-5861/$ – see front matter © 2004 Elsevier B.V. All rights reserved.
doi:10.1016/j.cattod.2004.08.010

[22]. Although, considerable research has been conducted on the immobilization of TiO_2 on adsorbents, detail characterization and performance evaluation of these catalysts in diverse applications are far from optimal. In addition, complete mineralization of the parent compound using TiO_2-adsorbent supported catalysts has seldom been reported in the literature.

In this work, TiO_2 photocatalysts supported on various adsorbents were developed, characterized and evaluated. Various adsorbents as catalyst support were selected based on the surface area and pore size. The supports used in this study are: (i) MCM-41, a mesoporous support with large surface area (>900 m^2/g), regular hexagonal array of uniform pores with pore sizes between 1.87 and 2.5 nm, (ii) β-zeolite (surface area 650–680 m^2/g) with pore sizes around 0.7 nm and (iii) Al-pillared montmorillonite (AlPC) with octahedral pillar of Al sandwiched between two tetrahedral silicate sheets (surface area 280–350 m^2/g). Catalysts were synthesized by a sol–gel method where ultra fine particles are formed. Orange II dye was chosen as the model compound to determine the photocatalyic efficiency of the supported catalysts in aqueous medium. The objective of this work is to compare the performances of the supported catalysts in degrading orange II under different operating conditions. In addition, the performances of these catalysts were also compared with those of bare TiO_2 prepared by sol–gel method and commercially available catalyst (Degussa-P25).

2. Experimental

2.1. Materials

Titanium tetra isopropoxide was purchased from Aldrich (Sigma–Aldrich, Germany), while orange II and azo dye were purchased from Sigma (Sigma–Aldrich, Germany). The analytical grade Al-pillared montmorillonite (Fluka), β-zeolite (Zeolyst International, UK, Si/Al = 20), Degussa-P25 (Degussa, Germany) were purchased and used without any purification. Pure siliceous MCM-41 was prepared in the lab following a method developed by Kawi et al. (2002) [23]. Analytical grade Aerosil, HCl (37%) (Merck, Germany), HNO_3 (65%) (Merck, Germany), NaOH pellets (Mallinckrodt AR., USA), CTMABr (Aldrich, Sigma–Aldrich, Germany) were used for the preparation of MCM-41 and the catalysts.

2.2. Synthesis of the catalysts

The TiO_2 sol was synthesized by acid catalyzed sol–gel formation method using 30 ml of 1 M HNO_3 and 7.4 ml of titanium tetra-isopropoxide following the hydrolysis reaction [24].

$$\mathrm{Ti\,(iso\text{-}OC_3H_7)_4 + 4H_2O \rightarrow Ti(OH)_4 + 4C_3H_7OH}$$

Titanium tetra-isopropoxide was added gradually to the aqueous solution of HNO_3 solution under continuous stirring for 1.5–2 h to produce a transparent sol containing 2 g of TiO_2 [25]. Subsequently, the colloid solution was diluted with de-ionized water and pH was adjusted to 3 with the addition of 1 M NaOH resulting in a turbid colloid. The pH adjustment was necessary to prevent the destruction of the structure of adsorbent due to reaction with acid. Depending on the (wt.%) loading of TiO_2 on the catalyst, requisite amount of adsorbent was added to the turbid colloid suspension. The resulting mixed suspension was agitated by magnetic stirrer for another 2 h at room temperature, followed by several centrifugations and washings with de-ionized water until the pH of the supernatant was about 6. The resulting supported TiO_2 catalyst was dried in an oven and subjected to calcination in furnace for 1 h at 300 °C. Finally the products were ground into fine powder and stored in dark. Catalysts supported on MCM-41, montmorillonite and β-zeolite were prepared with different TiO_2 contents (10, 25, 30, 40, 50, 60, and 80%). Bare TiO_2 without any support was also prepared using the above sol–gel technique.

2.3. Catalyst characterization

The synthesized catalysts were characterized using different analytical techniques. The nitrogen adsorption/desorption isotherm was obtained at liquid nitrogen temperature 77 K by using Quantachrome Autosorb1 automated gas adsorption system. The sample (0.1 g) was out-gassed for 6 h at 300 °C under vacuum before the analysis. The specific surface area was determined by using multi-point BET plot. The pore size and pore volume were determined by the BJH desorption isotherm.

The X-ray powder diffraction spectra of unsupported and supported TiO_2 were obtained using Shimadzu XRD-6000 powder diffractometer, where Cu target Kα-ray (operating at 40 kV and 30 mA, λ = 1.54059 Å) was used as the X-ray source. The scanning ranges 2θ = 1.5–10°, 5–50°, 10–80° were used to determine MCM-41, β-zeolite, montmorillonite and TiO_2 (both supported and unsupported catalysts), respectively.

Surface analysis of supported and unsupported TiO_2 catalysts was carried out by X-ray photoelectron spectroscopy (XPS) using high performance Kratos Axis analytical instrument HSI ESCA (electron spectroscopy for chemical analysis). Al Kα (1486.6 eV) X-rays were usually used for all the characterization. Binding energies (BE) for all the elements in the sample were calibrated relative to carbon impurity with a C 1s band at 248.7 eV.

Microscopic feature of supported and unsupported catalysts was obtained using scanning electron microscopy (SEM, JEOL JSM-5600LV) using fine catalyst powder supported on carbon tape and coated with platinum. Elemental analysis was performed with energy dispersive X-ray (EDX) spectroscopy.

2.4. Batch adsorption and photocatalytic experiments

Batch adsorption of orange II by TiO_2 supported on MCM-41, Al-pillared montmorillonite and β-zeolite was performed in a covered glass beaker fitted with a magnetic stirrer. Different initial concentrations of orange II ranging from 30–1000 ppm and different catalyst amounts (0.25, 0.5 and 1.0 g/l) were used. A total volume of 250 ml of orange II solution was used in the adsorption studies. In all experiments, ultrapure water (Milli Q plus 185, ultra pure water system) was used to make the solution.

The photocatalytic degradation of orange II in catalyst suspension was performed in a semi-batch swirl-flow reactor (63.5 ml) (Fig. 1). The reaction solution was introduced tangentially into the reactor from a reservoir (approximate volume = 250 ml) through a peristaltic pump. The flow rate of 310 ml/min was enough to eliminate the mass transfer limitation in the reactor [26]. The tangential introduction of the solution produced a swirl flow to mix the solution well. In addition, magnetic stirrer was used to induce good mixing of the solution into the reservoir. The temperature of the reservoir was maintained through a water jacket surrounding it. The experiments were conducted with dissolved oxygen saturation corresponding to ambient air, and no other additional oxidants were used.

In order to ensure dark adsorption, the solution was circulated through the reactor for about 1–2 h, prior to UV irradiation. A Phillips HPR 125 W high pressure mercury vapor lamp with a wavelength of 365 nm and an incident light intensity of 213 W/m^2 was used as the light source. During each run, the samples were taken from the reservoir at regular intervals and filtered to remove the catalyst with a Millex-VV filter (Millipore, 0.1 μm). Orange II concentration and TOC of the solution were measured by UV–vis spectrophotometer (UV-1601, Shimadzu) and a TOC analyzer (5000A, Shimadzu) with ASI-500 autosampler, respectively.

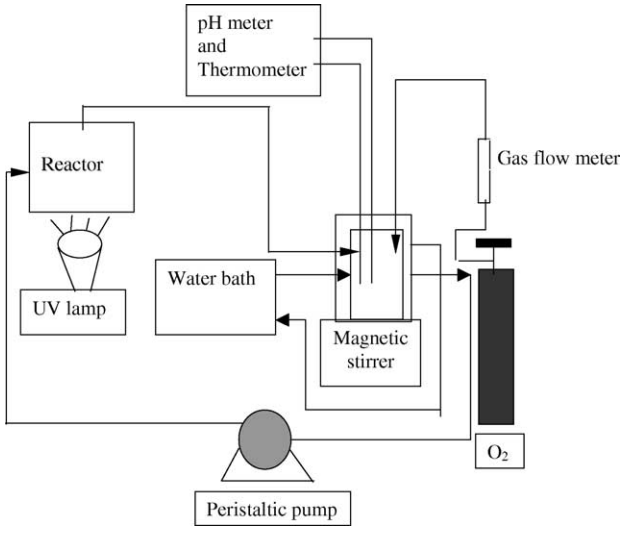

Fig. 1. A schematic diagram of the experimental setup.

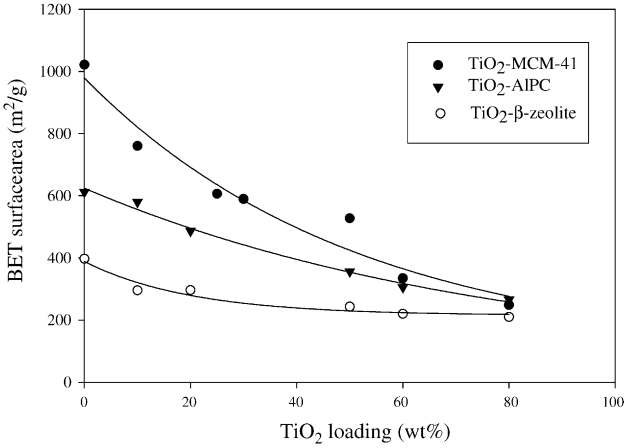

Fig. 2. BET surface area vs. TiO_2 (wt.%) loading on MCM-41, Al-pillared montmorillonite (AlPC) and β-zeolite.

3. Results and discussions

Based on the preliminary kinetic experiments, it was found that 50–60 wt.% TiO_2 on the adsorbents produced the best photodegradation rate of orange II (discussed later). Thus, in this paper some of the catalyst characterization results were reported mainly on 50 wt.% TiO_2.

3.1. Characterization of catalysts

3.1.1. BET analysis

The pore diameter, pore volume and specific surface area were determined using nitrogen adsorption/desorption isotherm and multi-point BET analysis. For all cases, with increasing loading of TiO_2, surface area of the supported catalysts on MCM-41, montmorillonite and β-zeolite decreased as shown in Fig. 2. The decrease in surface area is observed to be non-linear to the loading of TiO_2, indicating the adsorbent–TiO_2 is simply not a mechanical

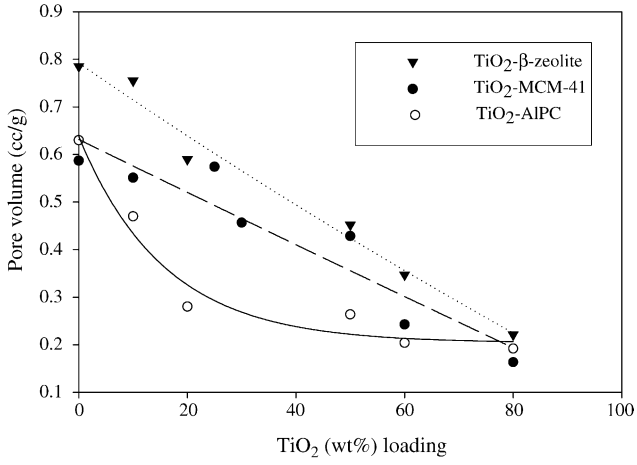

Fig. 3. Pore volume vs. TiO_2 (wt.%) loading on MCM-41, Al-pillared montmorillonite (AlPC) and β-zeolite.

mixture, rather titania has been dispersed inside the supports and causes partial blockage of the pores. Significant changes in the pore volume, especially for montmorillonite may suggest that TiO_2 was deposited inside the pores of the support (Fig. 3). BET surface areas of bare TiO_2 (160 m^2/g) prepared by sol–gel method and Degussa-P 25 (48 m^2/g) are much less than the supported TiO_2.

3.1.2. XRD analysis

X-ray powder diffraction method was used to assess the crystallinity of the catalyst particles. XRD peaks, characteristic of anatase were observed at $2\theta = 25.3^\circ$ [27] for both bare and supported TiO_2 on MCM-41, montmorillonite and β-zeolite (Fig. 4). Peaks corresponding to anatase TiO_2 also appeared at $2\theta = 37.8, 48.3, 54.8^\circ$. No significant peak of rutile was observed at $2\theta = 27.42^\circ$, although small peaks at 54.5° could be observed in some cases. As expected, with increasing TiO_2 (wt.%) loading, sharper peaks of TiO_2 were observed due to increased crystalline feature of TiO_2. Bare TiO_2 exhibits sharp peak characteristic indicating well-defined crystal of TiO_2 (shown in Fig. 4d). However, low intensity and broad peak characteristic of XRD spectrum of supported TiO_2 on MCM-41 and β-zeolite compared to that of bare TiO_2 indicate that highly dispersed fine particles of anatase TiO_2 were formed on these supports. On the other hand, XRD spectrum of TiO_2 supported on montmorillonite displays sharper TiO_2 peaks, indicating relatively larger TiO_2 crystallites formed on montmorillonite.

3.1.3. XPS analysis

The surface composition and chemical elementary state of all the catalysts were determined using XPS analysis. The binding energies of Ti (2p) of all three supported catalysts (Table 1) are essentially similar, which imply that Ti element for all the prepared catalysts exhibit similar state of oxidation and chemical environment. As expected, with the increased loading of TiO_2, the intensity of Ti ($2p_{3/2}$) for all the catalysts increased indicating greater coverage of the support surface by Ti. The binding energies of all the elements are in good agreement with the reported values

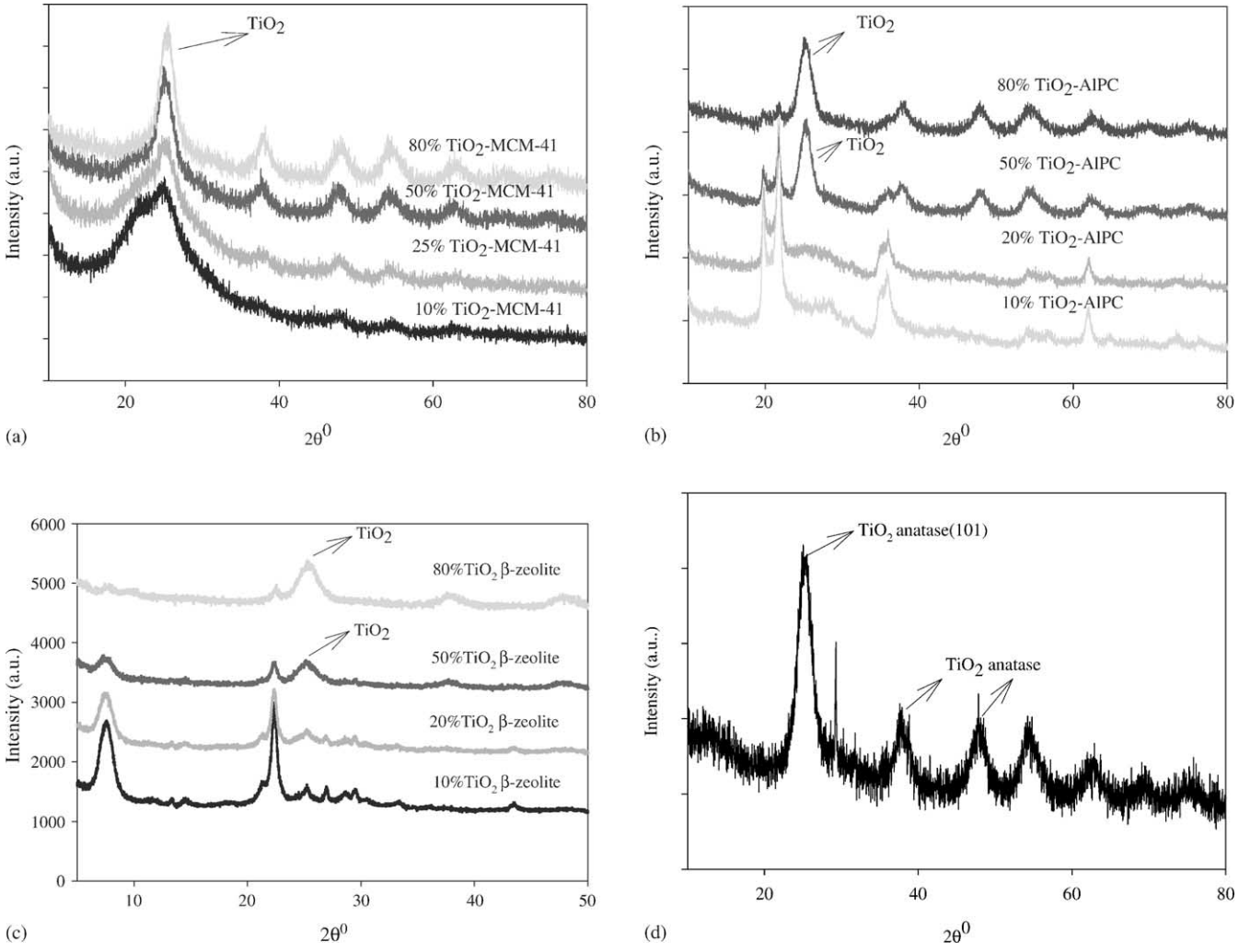

Fig. 4. XRD pattern of TiO_2 (wt.%) loaded on MCM-41 (a), Al-pillared montmorillonite (AlPC) (b), β-zeolite (c), and TiO_2 (sol–gel) (d).

Table 1
Binding energy of different elements present in TiO_2 catalysts

	Ti 2p (eV)	Si 2p (eV)	O 1s (eV)	Al 2p (eV)
Pure MCM-41	–	103.3	532.3	–
Pure AlPC[a]	–	103.2	531.9	74.8
Pure β-zeolite	–	103.3	531.9	73.9
10% TiO_2-MCM-41	458.5	103.1	532.0	–
25% TiO_2-MCM-41	458.5	102.9	532.4	–
50% TiO_2-MCM-41	458.6	103.1	532.0	–
80% TiO_2-MCM-41	458.7	102.5	531.8	–
10%TiO_2-AlPC[a]	458.5	102.8	531.9	74.4
20% TiO_2-AlPC[a]	458.5	102.7	531.9	74.7
50%TiO_2-AlPC[a]	458.7	102.3	531.3	73.9
80%TiO_2-AlPC[a]	458.5	102.1	532.1	75.0
10% TiO_2-β-zeolite	458.7	102.9	532.6	73.5
20% TiO_2-β-zeolite	458.5	102.8	532.8	73.6
50% TiO_2-β-zeolite	458.6	102.4	532.6	73.7
80% TiO_2-β-zeolite	458.7	102.3	532.5	73.3
TiO_2 (sol–gel)	458.9	–	532.6	–

[a] AlPC represents Al-pillared montmorillonite.

[8,28,29,30]. Comparing the reported binding energies, the oxidation state of Ti corresponds to both tetrahedral and octahedral coordinated Ti.

3.1.4. SEM-EDX analysis

Morphology of the supports and the supported catalysts were determined using SEM micrographs. It can be seen from Fig. 5a that pure MCM-41 did not exhibit well-defined crystalline feature while Al-pillared montmorillonite exhibited layered crystalline structure (Fig. 5c), and pure β-zeolite shows both spherical and rhombic crystals (Fig. 5e). SEM coupled with an EDX microprobe furnished a semi-quantitative elemental analysis of the surface indicating that Ti was present over almost all part of the supports (Fig. 5f and i–k). However, SEM micrographs shown in Fig. 5b, d and f do not clearly display the crystallites of TiO_2 indicating the formation of fine particles of TiO_2 on the support. Comparatively bigger crystals were formed for bare TiO_2 prepared by the sol–gel method (Fig. 5g).

3.2. Batch adsorption and photodegradation study

It is imperative that the adsorption characteristics of the supported catalysts are better than that of bare TiO_2. As mentioned earlier, initial photodegradation experiments indicated that about 50 wt.% TiO_2 loading on adsorbent produces the best photodegradation rates. Thus, in this paper all the adsorption and photodegradation results are presented with the catalysts with 50 wt.% loading of TiO_2.

Adsorption isotherm results of orange II for different supported and unsupported catalysts are shown in Fig. 6, where all the supported catalysts showed very good adsorption characteristics compared to that of bare TiO_2, and Degussa-P25. However, interestingly pure supports with very high surface areas show very poor adsorption of orange II. Orange II being slightly acidic and anionic is subjected to electrostatic repulsion between it and the negative surface of the supports. Adsorption increased only with the increasing loading of TiO_2 with maximum adsorption occurring at 50–60 wt.% loading of TiO_2. The following surface reaction for the supported catalysts is expected to occur below pH 6.8 (pzc of TiO_2):

$$Ti - OH + H^+ \leftrightarrow TiOH_2^+$$

In this case, adsorption of orange II is facilitated due to the electrostatic attraction between the anionic dye and positively charged TiO_2 on the surface. However, with the increased loading of TiO_2 (beyond 50–60%) the surface area of the catalysts decreases, thus eventually leading to lower adsorption indicating the presence of optimal loading. Incidentally, despite lower surface area of TiO_2-montmorillonite catalysts compared to that of TiO_2 supported on MCM-41 and β-zeolite, orange II exhibited stronger adsorption characteristics for TiO_2-montmorillonite (Fig. 6). The factors that can attribute to the preferential adsorption of orange II on TiO_2-montmorillonite are: (i) interlayer surface of the pillared clay is hydrophobic and facilitate the adsorption of organics, and (ii) shape selectivity because of its pore structure.

Prior to the actual photodegradation experiments, blank photodegradation experiments were conducted using pure MCM-41, montmorillonite and β-zeolite (Fig. 7). As expected, there was no significant removal of orange II when the UV-radiation was applied to the solution. These experiments were essential in order to establish the photodegradation efficiency of the TiO_2 catalysts supported on adsorbents over the only adsorption by the adsorbents. It should be noticed that the UV-light was turned on only when the adsorption equilibrium was attained for a certain initial concentration of orange II. It also indicates that the pure adsorbents never participated in the photodegradation of orange II. These experiments also indicate that direct photolysis of orange II is negligible.

The dark adsorption experiments involving all the catalysts indicate that effective surface area and adsorption capacity of the supported TiO_2 were much higher than that of bare TiO_2, and Degussa-P25, which favor rapid removal of orange II from the solution (Fig. 8). Consequently, overall removal of orange II by TiO_2 supported on adsorbent was considerably higher than that of bare TiO_2 and the Degussa-P25 (Fig. 9). All experiments were performed under natural pH condition (pH 4.14–4.54) using 50 ppm of orange II, and 0.5 g/l of catalyst. As mentioned earlier, among the different loadings (10–80 wt.%) of TiO_2 on the support, catalysts with about 50 wt.% TiO_2 loading performed the best indicating the presence of an optimal amount of TiO_2. At lower loading of TiO_2, the overall reaction rate is dictated by the surface reaction, while at higher loading, the extent of adsorption limits the overall reaction.

The rate of degradation on the supported TiO_2 catalysts depends on the initial concentration of orange II, and

followed Langmuir–Hinshelwood model in the following form:

$$r_0 = \frac{kK_eC_0}{1 + K_eC_0}$$

At high initial concentration, the reaction rate followed zero order reaction with respect to orange II concentration. The initial rate and apparent half-life ($t_{1/2}$) of orange II for all the catalysts are presented in Table 2. The performances of TiO_2-β-zeolite and TiO_2-MCM-41 were better than Degussa-P25, while TiO_2-montmorillonite shows significantly lower reaction rate than Degussa-P25. Too strong adsorption would hinder the mobility of the adsorbed substrate to the photoactive TiO_2 sites as was found in the case of TiO_2-loaded on activated carbon [31]. Although, TiO_2-montmorillonite did not exhibit very good photocatalytic efficiency, overall removal of orange II is much better by TiO_2-montmorillonite than bare TiO_2 due to initial lowering of peak concentration of orange II owing to adsorption (can be seen in the half-life shown in Table 2).

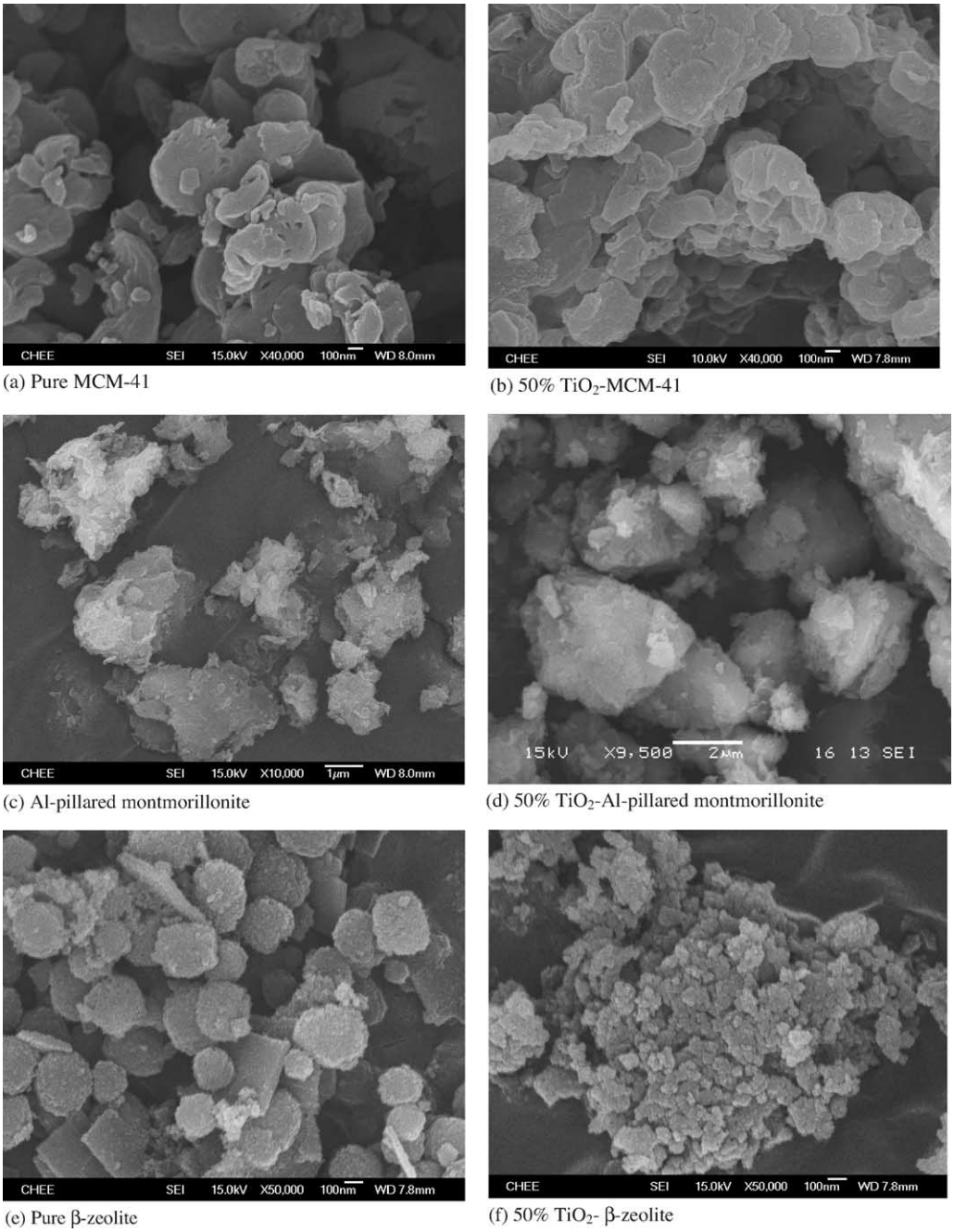

(a) Pure MCM-41
(b) 50% TiO_2-MCM-41
(c) Al-pillared montmorillonite
(d) 50% TiO_2-Al-pillared montmorillonite
(e) Pure β-zeolite
(f) 50% TiO_2- β-zeolite

Fig. 5. SEM of pure MCM-41 (a), 50% TiO_2-MCM-41 (b), pure Al-pillared montmorillonite (c), 50% TiO_2-Al-pillared montmorillonite (d), pure β-zeolite (e), 50% TiO_2-β-zeloite (f), TiO_2 (sol–gel) (g), EDX of TiO2 (sol–gel) (h), 50% TiO_2-MCM-41 (i), 50% TiO_2-Al-pillared montmorillonite (j), and 50% TiO_2-β-zeloite (k).

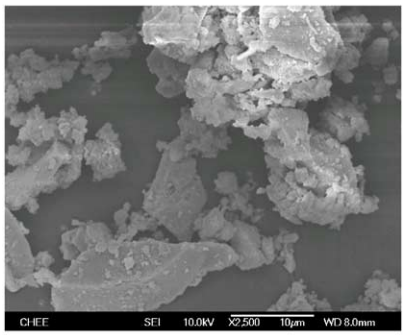

(g) TiO_2 (sol-gel)

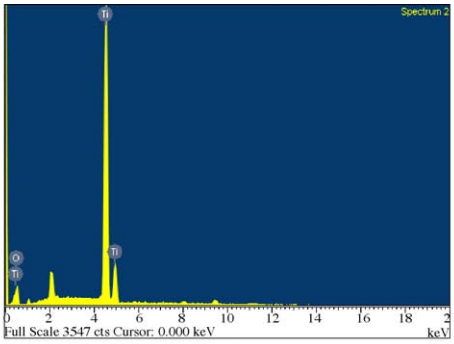

(h) EDX of TiO_2 (sol-gel)

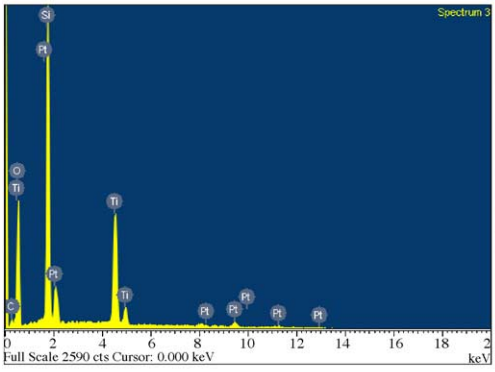

(i) EDX of 50% TiO_2-MCM-41

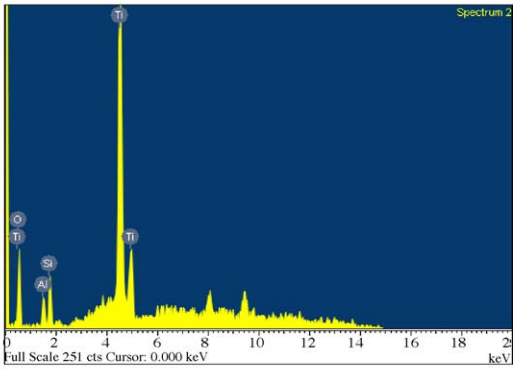

(j) EDX of 50% TiO_2-Al-pillared montmorillonite

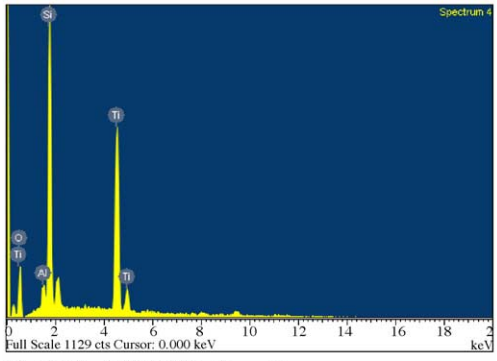

(k) EDX of 50% TiO_2-β-zeolite

Fig. 5. (*Continued*).

The crystallite structure of anatase plays key role in the photodegardation of organics. Earlier, SEM analysis had shown that the degree of crystallinity of the anatase deposited on all three supports for 50 wt.% loading of TiO_2 was comparable. In addition, XPS analysis also indicated that the chemical environments (oxidation state) of deposited TiO_2 on various supports were also very similar. The TiO_2 formed on supported catalyst indicated much finer particles than bare TiO_2 prepared by sol–gel method. Finer particles show greater photocatalytic efficiency by providing greater driving force for charge transfer existed in quantum sized TiO_2 semiconductor particles [11].

Although, the supported catalysts were very efficient in the degradation of orange II, complete mineralization was much slower as indicated by the TOC analysis of the solution. Typically, it took about 3 h for complete decoloration of the solution, and the concentration of orange II to reach below detection limit from an initial concentration of 50 ppm, while only 10–20% of the TOC reduced by that time. However, TOC reduction dramatically improved when external ozone was added to the solution (TOC goes below 5 ppm within 120 min of radiation for all the catalysts). Since orange II is adsorbed on the catalyst surface by electrostatic attraction, it is expected that photodegradation takes place at the surface of the catalyst. A rapid exchange of the photoactive species to the reactive surface is essential for complete mineralization. However, the intermediates formed by the photodegradation of orange II are probably strongly adsorbed on the supports inhibiting complete mineralization. The rupture at the N=N bond

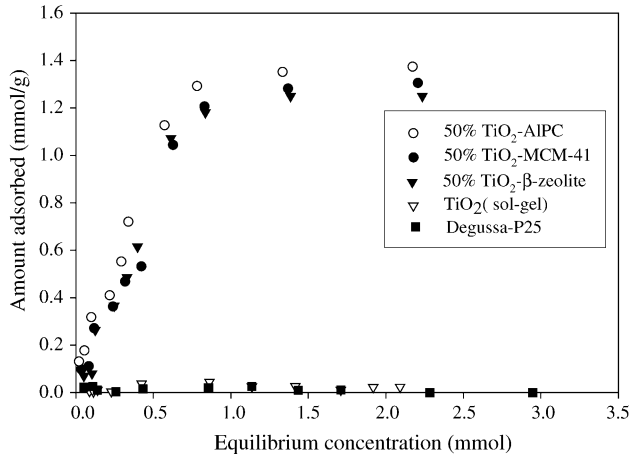

Fig. 6. Adsorption equilibrium of orange II for different 50 wt.% TiO_2-loaded catalysts, Degussa-P25 and TiO_2 prepared by sol–gel (catalyst concentration = 0.5 g/l, concentration of orange II varies from 30–1000 ppm, natural pH, calcination temperature = 300 °C).

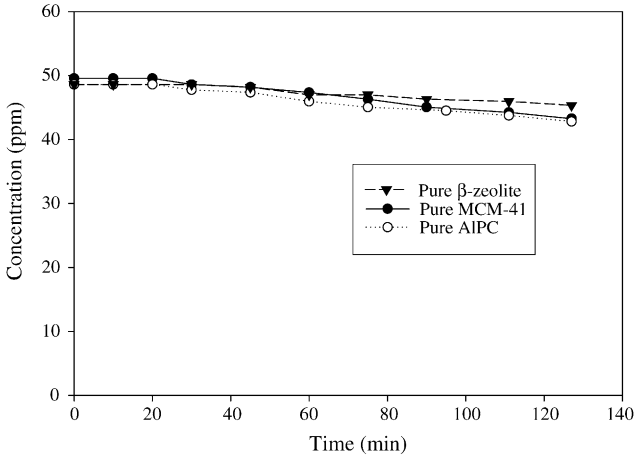

Fig. 7. Photodegradation of orange II by different supports (catalyst concentration = 0.5 g/l, initial concentration of orange II = 50 ppm, natural pH).

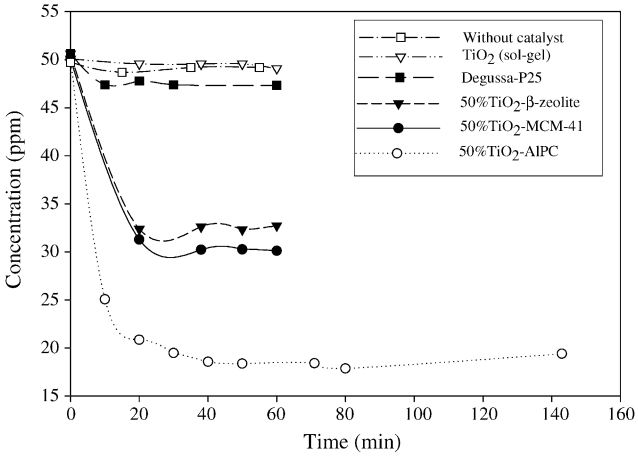

Fig. 8. Dark adsorption of orange II by 50 wt.% TiO_2-loaded catalysts, Degussa-P25 and TiO_2 prepared by sol–gel and without any catalyst (catalyst concentration = 0.5 g/l, initial concentration of orange II = 50 ppm, natural pH, calcination temperature = 300 °C).

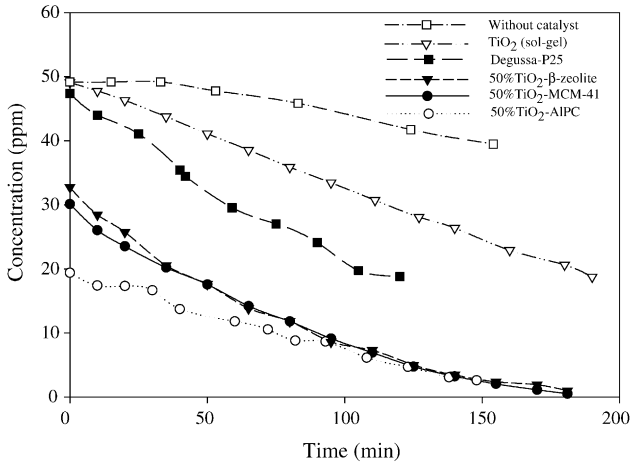

Fig. 9. Photodegradation of orange II by 50 wt.% TiO_2-loaded catalysts, Degussa-P25 and TiO_2 prepared by sol–gel and without any catalyst (catalyst concentration = 0.5 g/l, initial concentration of orange II = 50 ppm, natural pH, calcination temperature = 300 °C).

Table 2
Initial rate and half-life of orange II for different catalysts

Catalyst	Initial rate (ppm/min)	$t_{1/2}$ (min)
50% TiO_2-MCM-41	0.400	70
50% TiO_2-AlPC[a]	0.093	75
50% TiO_2-β-zeolite	0.431	65
Degussa-P25	0.334	87
TiO_2 sol–gel	0.131	140

[a] AlPC represents Al-pillared montmorillonite.

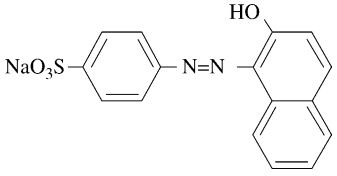

Fig. 10. Chemical structure of orange II.

(structure shown in Fig. 10) will lead to the formation of benzene and naphthalene rings followed by a myriad of intermediates such as phenol, oxalate, malonate, etc. [32,33] whose anions would also be strongly adsorbed on the surface based on pH. Formation of dibutyl phthalate was confirmed by continuous scanning of the reaction medium during photooxidation of orange II using UV-spectrophotometer when an additional absorbance peak at 260–300 nm occurred and height of this peak increased, while the peak absorbance of orange II at 484 nm decreased with time. The initial natural pH (4.1–4.5) of the solution decreased during the photodegradation experiment and the final pH varied from 3.8 to 4.2 depending on the supported catalysts used in the experiment. Thus, the kind of adsorbent, and subsequently TiO_2-adsorbent, which would yield the highest activity depends on the target organic compound.

4. Conclusions

Photocatalytic efficiency of supported TiO_2 catalyst on three types of adsorbents was compared with that of bare TiO_2 produced by sol–gel method and commercially available Degussa-P25 catalyst. The supported catalysts effectively removed an azo-dye orange II from solution, and the rate of degradation was significantly better than that of bare TiO_2 (sol–gel) and Degussa-P25. The performance improvement can be attributed to the high surface areas of the adsorbent used, crystallinity and particle size of deposited TiO_2. All three supported catalysts exhibited comparable overall removal efficiency of orange II, although TiO_2-MCM-41 and TiO_2-β-zeolite were better photocatalysts than TiO_2-montmorillonite, while adsorption of orange II was maximum on TiO_2-montmorillonite. The performance of the supported catalysts will depend significantly on the nature of the substrate used.

References

[1] D.F. Ollis, H. Al-Ekabi (Eds.), Photocatalytic Purification and Treatment of Water and Air, Elsevier, Amsterdam, 1993.
[2] N. Serpone, E. Pelizzetti (Eds.), Photocatalysis, Fundamentals and Applications, Wiley, New York, 1989.
[3] M. Schiavello, Photocatalysis and Environment, Kluwer, Dordecht, 1988.
[4] T. Torimoto, Y. Okawa, N. Takeda, H. Yoneyama, J. Photochem. Photobiol. A: Chem. 103 (1997) 153.
[5] Y. Xu, C.H. Langford, J. Phys. Chem. 99 (1995) 11501.
[6] G.P. Lepore, L. Persaud, C.H. Langford, J. Photochem. Photobiol. A: Chem. 98 (1996) 103.
[7] Y. Xu, C.H. Langford, J. Phys. Chem. B 101 (1997) 3115.
[8] M. Anpo, H. Nakaya, S. Kodama, Y. Kubokawa, J. Phys. Chem. 90 (1986) 1633.
[9] C. Anderson, A.J. Bard, J. Phys. Chem. 99 (1995) 9882.
[10] G.P. Lepore, L. Persaud, C.H. Langford, J. Photochem. Photobiol. A: Chem. 98 (1996) 103.
[11] Y. Xu, W. Zheng, W. Liu, J. Photochem. Photobiol. A: Chem. 122 (1999) 57.
[12] C. Minero, F. Catozzo, E. Pelizzetti, Langmuir 8 (1992) 481.
[13] C. Anderson, A.J. Bard, J. Phys. Chem. B 101 (1997) 2611.
[14] T. Torimoto, Y. Okawa, N. Takeda, H. Yoneyama, J. Photochem. Photobiol. A: Chem. 103 (1997) 153.
[15] J. Hermann, J. Matos, J. Disdier, C. Guillard, J. Laine, S. Malato, J. Blanco, Catal. Today 54 (1999) 255–265.
[16] H. Yoneyama, T. Torimoto, Catal. Today 58 (2000) 133.
[17] J.F. Tanguay, S. Suib, R.W. Coughlin, J. Catal. 117 (1989) 335.
[18] S. Sampath, H. Uchida, H. Yoneyama, J. Catal. 149 (1994) 189.
[19] K. Shimizu, T. Kaneko, T. Fujishima, T. Kodama, H. Yoshida, Y. Kitayama, Appl. Catal. A: Gen. 225 (2002) 185.
[20] C. Anderson, A.J. Bard, J. Phys. Chem. 99 (1995) 9882.
[21] N. Takeda, M. Ohtani, T. Torimoto, S. Kuwabata, H. Yoneyama, J. Phys. Chem. 101 (1997) 2644.
[22] J.M. Lopez Nieto, Top. Catal. 15 (2001) 189.
[23] S. Kawi, S.C. Shen, P.L. Chew, J. Mater. Chem. 12 (2002) 1582.
[24] M.A. Anderson, M.J. Gisselman, Q. Xu, J. Membr. Sci. 39 (1988) 243.
[25] N. Takeda, T. Torimoto, S. Sampath, S. Kuwabata, H. Yoneyama, J. Phys. Chem. 99 (1995) 9986.
[26] K. Mehrotra, G.S. Yablonsky, A.K. Ray, Ind. Eng. Chem. Res. 42 (2003) 2273.
[27] J. Liqiang, S. Xiaojun, C. Weimin, X. Zili, D. Yaoguo, J. Phys. Chem. Solids 64 (2003) 615.
[28] T. Blasco, M.A. Camblor, J.L.G. Fierro, J. Pérez-Pariente, Microporous Mater. 3 (1994) 259.
[29] B.M. Reddy, B. Chowdhuri, E.P. Reddy, A. Fernández, Appl. Catal. A: Gen. 213 (2001) 279.
[30] H. Yasuyuki, A. Ayame, Catal. Today 71 (2001) 177.
[31] H. Yoneyama, T. Torimoto, Catal. Today 58 (2000) 133.
[32] M. Neamtu, I. Siminiceanu, A. Yediler, A. Kettrup, Dyes Pigments 53 (2002) 93.
[33] V. Augugliaro, C. Baiocchi, A.B. Prevot, E. Garacía-López, V. Loddo, S. Malato, G. Marcí, L. Palamisano, M. Pazzi, E. Pramauro, Chemosphere 49 (2002) 1223.